Performance of precast concrete moment frames subjected to column removal: Part 1, experimental study

H. S. Lew, Joseph A. Main, Yihai Bao, Fahim Sadek, Vincent P. Chiarito, Stephen D. Robert, and Jorge O. Torres

- This paper presents a full-scale experimental study of two precast concrete moment-frame assemblies (one ordinary and the other special) representing portions of seismically designed perimeter moment frames from two 10-story prototype buildings.

- The assemblies were subjected to monotonically increasing vertical displacement of the unsupported center column to observe their behavior and failure modes under simulated column removal.

- The failures of both the ordinary moment frame and special moment frame specimens were characterized by fractures of the bottom anchorage bars at the welded connection to the center column and diagonal cracking and shear deformation of the end columns under outward forces generated by arching action in the beams.

On May 16, 1968, a gas explosion blew out a load-bearing exterior wall on the 18th floor of the Ronan Point tower block in London, U.K., causing a progression of failures that resulted in the collapse of an entire corner of the 22-story precast concrete building.[1,2] This event provided an impetus for extensive research on the collapse resistance of large-panel precast concrete structures and for the development of design approaches for various structural systems to prevent such cases of disproportionate collapse. Elliott and Jolly[3] present a review of previous experimental research on collapse resistance of precast concrete structures and a summary of design approaches for disproportionate collapse mitigation with application to multistory precast concrete structures. One such approach is the tie force method, an indirect design approach that requires minimum levels of strength and continuity in the connections between the various components of a structure. However, this approach does not consider the ductility of the ties and, thus, does not ensure that the loads can actually be redistributed as large deformations develop following a local failure. The alternative load path method is a direct design approach that requires structural analysis to demonstrate explicitly the adequacy of the structural system to redistribute loads following a local failure. This approach requires characterization of the nonlinear behavior and ductility of structural components and connections.

Experimental data from structural assemblies and systems under local failure scenarios, such as column removal, are indispensable in characterizing the complex nonlinear behaviors whereby alternative load paths can be developed. Experimental data are also critical for the validation of models used to represent such behaviors in the analysis of structural systems.

To address the need for such experimental data and associated modeling capabilities, the National Institute of Standards and Technology (NIST) is conducting a comprehensive analytical and experimental research program to study the vulnerability of multistory building structures to disproportionate collapse. As part of this research, 10-story prototype buildings have been designed with various structural systems, including steel-frame, cast-in-place concrete–frame, and precast concrete–frame buildings. Moment-frame assemblies representing portions of these structural systems have been tested at full scale under simulated column removal. Sadek et al.[4] described testing and analysis of steel moment-frame assemblies, while Lew et al.[5] described testing and analysis of cast-in-place concrete moment-frame assemblies. This paper focuses on testing of precast concrete moment-frame assemblies, while a companion paper[6] presents computational modeling and analysis of these test specimens.

Experimental data on the disproportionate collapse resistance of precast concrete moment-resisting–frame structures is limited. As summarized by Elliott and Jolly,[3] several experimental studies have investigated the effectiveness of tie forces in precast concrete floor slabs at redistributing loads through catenary action.[7–9] Recently, Nimse et al.[10,11]

tested one-third-scale precast concrete frame assemblies under a column removal scenario, comparing the performance of monolithic connections; cast-in-place concrete, or wet, connections; and field-bolted, or dry, connections. Kang and Tan[12] performed testing of half-scale precast concrete frame assemblies with cast-in-place concrete connections under simulated column removal, comparing the performance of specimens with different reinforcement details in the joints. These recent reduced-scale assembly tests[10–12] considered rectangular beams with clear span-to-depth ratios of approximately nine, which is comparable to the clear span-to-depth ratio of beams in the cast-in-place concrete assemblies tested previously by Lew et al.[5]

The study reported herein included full-scale testing of two precast concrete moment-frame assemblies, each comprising three columns and two beams. Although both specimens had moment-resisting beam-to-column connections, one specimen was designed as part of an ordinary moment frame and the other was designed as part of a special moment frame. The specimens were subjected to displacement-controlled vertical loading of the unsupported center column to observe their behavior under a simulated column removal scenario, including the development of flexural action and arching action. Each test was continued beyond the ultimate capacity of the assembly to characterize the failure modes and collapse mechanisms that developed.

Design of prototype buildings

NIST, working with a panel of experts that included practicing structural engineers and fabricators, developed the overall configuration and dimensions of two prototype
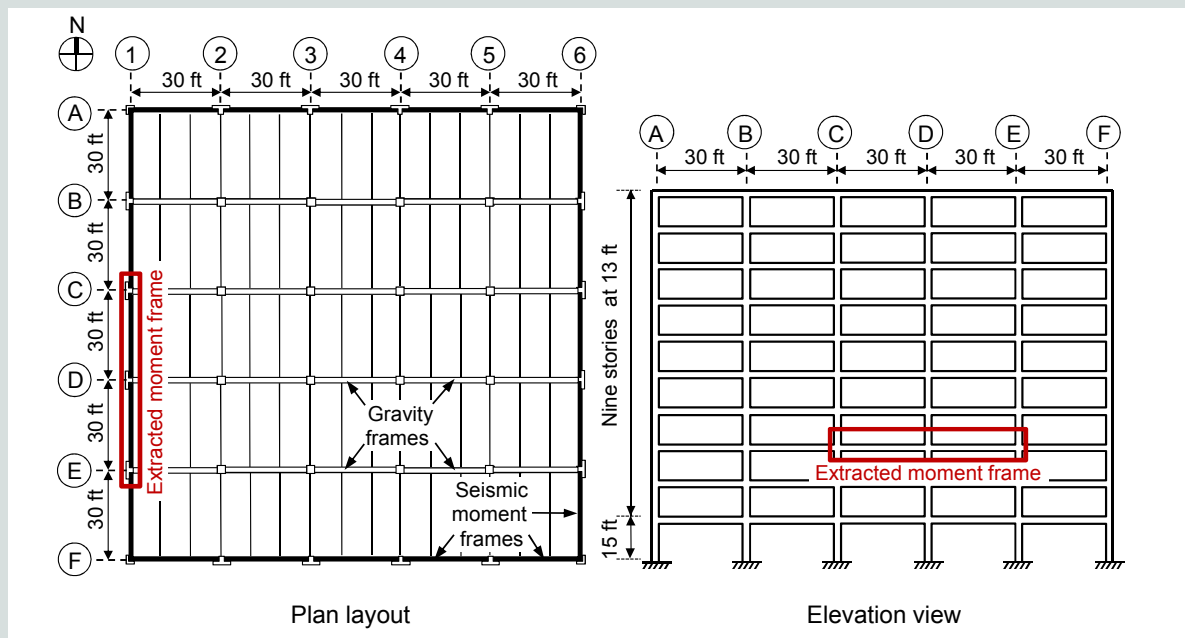
Figure 1. Prototype buildings. Note: 1 ft = 0.305 m.
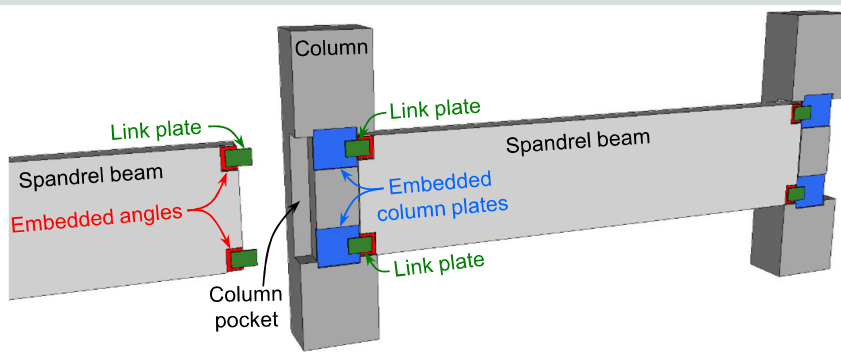
Figure 2. Perspective illustration of a perimeter moment frame showing link-plate connections and placement of spandrel beams within pockets in the columns.

10-story precast concrete buildings for office occupancy. The design of the buildings is described in NIST Technical Note 1886.[13] To examine the effectiveness of seismic design and detailing in resisting disproportionate collapse, alternative designs were developed for seismic design categories B and D. A square plan layout was chosen for both prototype buildings (**Fig. 1**), with plan dimensions of 150 × 150 ft (46 × 46 m). Both buildings have perimeter moment frames designed to resist lateral loads, while the interior framing was designed for gravity loads only. The building designed for seismic design category B incorporates ordinary moment frames, while the building designed for seismic design category D incorporates special moment frames. The interior gravity framing consists of simply supported inverted T beams spanning between columns in the east-west direction. The floor system consists of cambered double-tee members spanning the north-south direction, with a concrete topping that varies in thickness from 3.5 in. (89 mm) over the inverted T beams to 2.5 in. (64 mm) at midspan of the double-tee members.

The spandrel beams in the perimeter moment frames were placed inside pockets in the exterior columns (**Fig. 2**), and moment connections were established by welding steel link plates to steel angles embedded in the beams and to steel plates embedded in the columns. **Figure 3** shows the special moment frame connection details. The ordinary moment frame connections were similar but with two no. 10 (32M) anchorage bars per link plate and different dimensions of the components. Details are provided in NIST Technical Note 1886.[13] The steel column plates were embedded in the column concrete using AWS D1.1 Type B headed studs.[14] Anchorage reinforcing bars in the spandrel beams were welded to the steel angles embedded at the top and bottom of the beams. The beam moment was transferred to the column by the coupling forces generated in the top and the bottom link plates. Torsional restraint for the spandrel beams was provided by torsion rods installed through sleeves in the beams and columns. For both the ordinary moment

frame and special moment frame connections, Class B splices were provided between the anchorage bars and the beam flexural reinforcement to maintain continuity of the beam reinforcement through the connection, as required for precast concrete special moment frames in section 21.6.2 of the American Concrete Institute's (ACI's) *Building Code Requirements for Structural Concrete (ACI 318-05) and Commentary (ACI 318R-05)*.[15]

The precast concrete special moment frames were designed in accordance with sections 21.2 through 21.6 of ACI 318-05. As noted in section 3.6.4 of the *PCI Design Handbook: Precast and Prestressed Concrete*,[16] these provisions aim to produce structures with strong column, weak beam behavior. Section 21.3 of ACI 318-05 specifically requires that flexural members of special moment frames have a clear span not smaller than four times the effective depth. To comply with this requirement, the special moment frame spandrel beams had a reduced depth relative to the ordinary moment frame spandrel beams. The clear span–to–depth ratio was 2.7 for the ordinary moment frame spandrel beams and 4.2 for the special moment frame spandrel beams. Cross-sectional dimensions and reinforcement details of the beams and columns are presented subsequently.

The prototype buildings were designed according to ASCE 7-05[17] for occupancy category II. Seismic design of the ordinary moment frame building was based on a location in Atlanta, Ga., on Site Class C. Seismic design of the special moment frame building was based on a location in Seattle, Wash., on Site Class D. Both the precast concrete structural members and the concrete topping were designed using normalweight concrete, with a density of 150 lb/ft^3 (24 kN/m^3). A compressive strength of 6000 psi (41 MPa) was specified for the precast concrete structural members, and a compressive strength of 4000 psi (28 MPa) was specified for the concrete topping. A minimum yield strength f_y of 60 ksi (410 MPa) was specified for the reinforcing bars.

Experimental program

The primary objectives of these tests were the following:

- to characterize the response of the precast concrete moment frames under a column removal scenario, particularly the capacity of the moment connections to transfer loads through flexural action and other mechanisms

- to provide experimental data for validation of finite-element models to be used in evaluating the robustness of precast concrete structural systems

The test specimens were two-span moment-frame assemblies extracted from the third-floor framing system in the north-south direction (C1~E1) of the 10-story buildings (Fig. 1). The specimen from the seismic design category B building was part of an ordinary moment frame, while the specimen from the seismic design category D building was part of a special moment frame.

Experimental configuration

Figure 4 illustrates the experimental configuration, which was essentially the same for both specimens and is further described in NIST Technical Note 1886.[13] The span length of the test specimens was reduced from 30 ft (9.1 m) to 25 ft (7.6 m) to fit within the testing facility. The effect of the shortened span length was evaluated using computational modeling and is discussed in the companion paper.[6]

The tops of the end columns were restrained by a steel frame to simulate the bracing effect provided by the upper stories in a multistory building. Vertical load was applied to the unsupported center column using a hydraulic actuator with a capacity of 400 kip (1800 kN) and a stroke of 20 in. (510 mm). The load was applied under displacement control at a rate of 1 in./min (25 mm/min). Horizontal movements of the steel loading plate were restrained by four columns positioned at the corners of the plate (Fig. 5). A special roller bearing support arrangement at the four corners of the plate allowed free vertical displacement of the plate along the four columns. Lateral bracing was provided at the lower end of the center column and at the midspan of each beam (Fig. 4).

Test specimens

Figure 5 shows member sizes and reinforcement details for the ordinary moment frame and special moment frame specimens. The columns had a rectangular cross section (section AA in Fig. 4), which was reduced to a T shape in the connection regions to form pockets for the spandrel beams (section BB in Fig. 4). Column longitudinal reinforcing bars were welded to 1 in. (25 mm) thick steel plates

at the bases of the end columns. The front of each specimen denotes the surface on which the link plates were welded when making the moment connections, and the designations left beam and right beam correspond to the orientation of the beams when viewing the specimen from the front (Fig. 4).

The beams of the special moment frame specimen were inadvertently installed in an inverted orientation so that the longer anchorage bars were at the bottom of the beams rather than at the top as designed (Fig. 3). A slight misalignment of the torsion rod sleeves in the beams and columns also prevented installation of the torsion rods for the special moment frame specimen. As discussed in NIST Technical Note 1886,[13] the implications of these errors were investigated using computational modeling and were found to have only a slight influence on the response of the special moment frame specimen. The experimental results obtained for the special moment frame specimen are therefore believed to represent quite closely the behavior of the specimen as designed.

Measured material properties of the concrete and ASTM A706 Grade 60 reinforcing bars[18] are reported in NIST Technical Note 1886.[13] The average measured 28-day compressive strength of concrete was 5785 psi (39.89 MPa), and the average 28-day splitting tensile strength of concrete was 469 psi (3.23 MPa). All plates and angles were made of ASTM A36 steel[19] with a minimum specified yield strength of 36 ksi (250 MPa). The torsion rods were ASTM A193 Grade B7 bolts[20] with a minimum tensile strength of 125 ksi (862 MPa).

Instrumentation

The complete instrumentation systems for the two test specimens are described in NIST Technical Note 1886.[13] A total of 67 channels of data were recorded for the ordinary moment frame specimen, and 77 channels of data were recorded for the special moment frame specimen. Displacement measurements included vertical displacements of the center column and the beams and horizontal displacements of the end columns. Two types of transducers were used to measure displacements: spring-loaded, string-type displacement potentiometers with a range of 72 in. (1830 mm) and an accuracy of 0.001 in. (0.025 mm) and linear variable differential transformers (LVDTs) with a range of 6 in. (150 mm) and an accuracy of 0.005 in. (0.13 mm). LVDTs were used only to measure horizontal displacements of the end columns for the ordinary moment frame specimen, while all other displacements were measured using string potentiometers. To measure the rotation of the beam ends, digital inclinometers were attached to the top surface of the beams.

Both specimens were extensively instrumented with electrical resistance strain gauges attached to the surfaces of selected steel components. Uniaxial strain gauges were
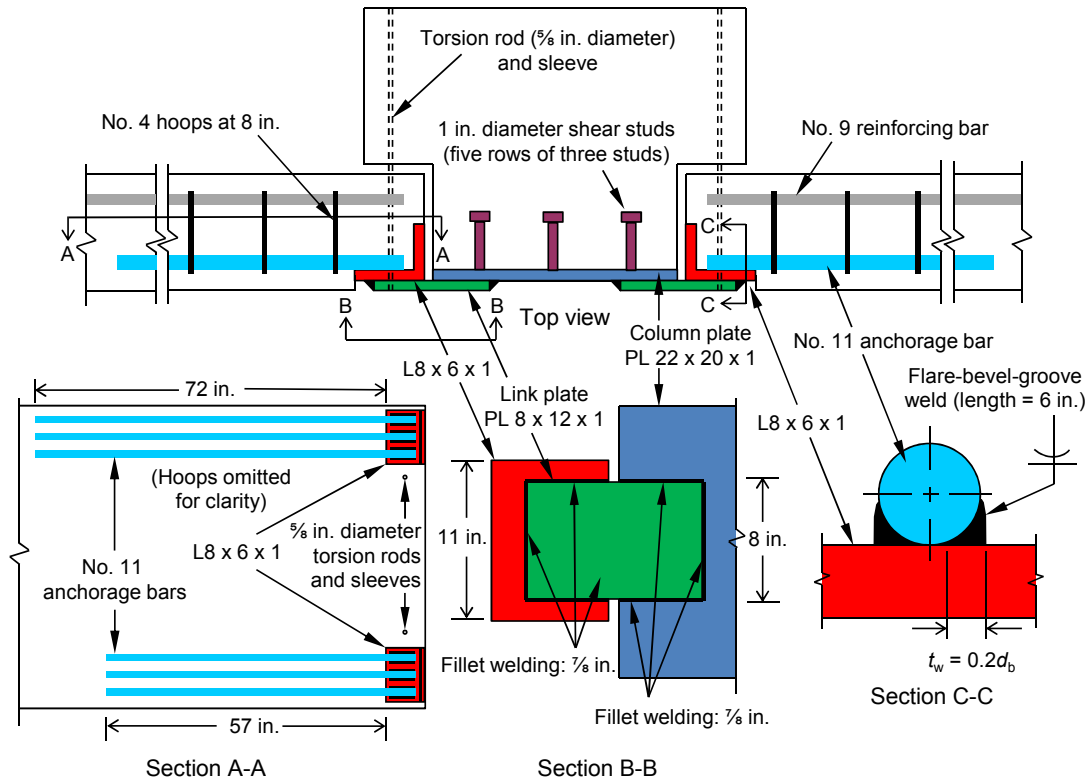
Figure 3. Special moment frame connection details. Note: d_b = reinforcing bar diameter = 1.41 in.; t_w = throat dimension of flare-bevel-groove weld = 0.28 in. No. 4 = 13M; no. 9 = 29M; no. 11 = 36M; L8 × 6 × 1 = L200 × 150 × 25; PL8 × 12 × 1 = PL200 × 300 × 25; PL22 × 20 × 1 = PL560 × 510 × 25; 1 in. = 25.4 mm.
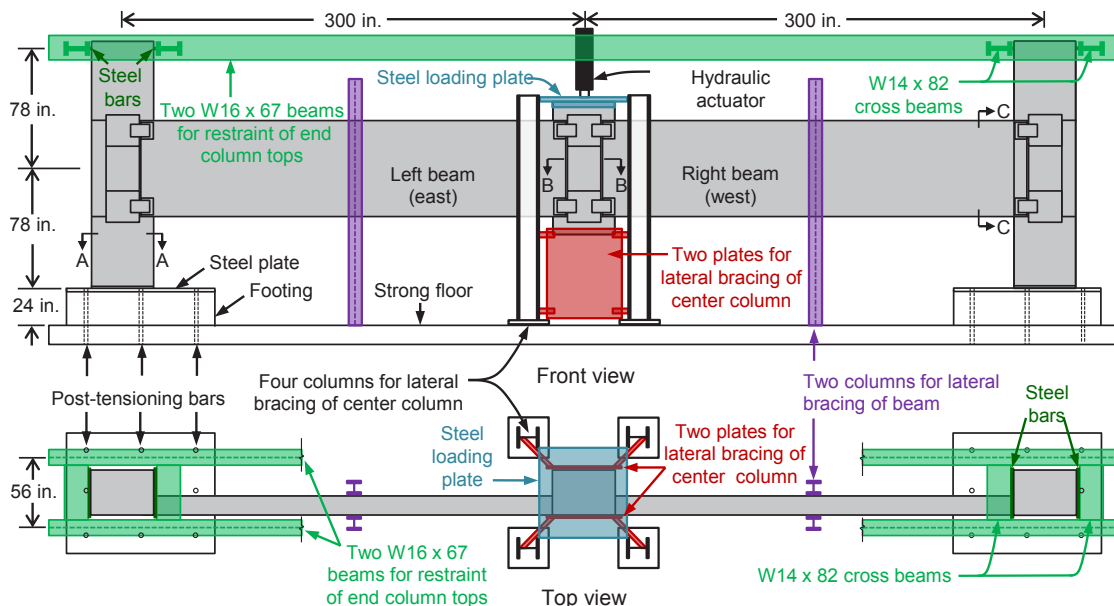
Figure 4. Front and top views of experimental configuration. Note: W14 × 82 = W360 × 120; W16 × 67 = W410 × 100; 1 in. = 25.4 mm.
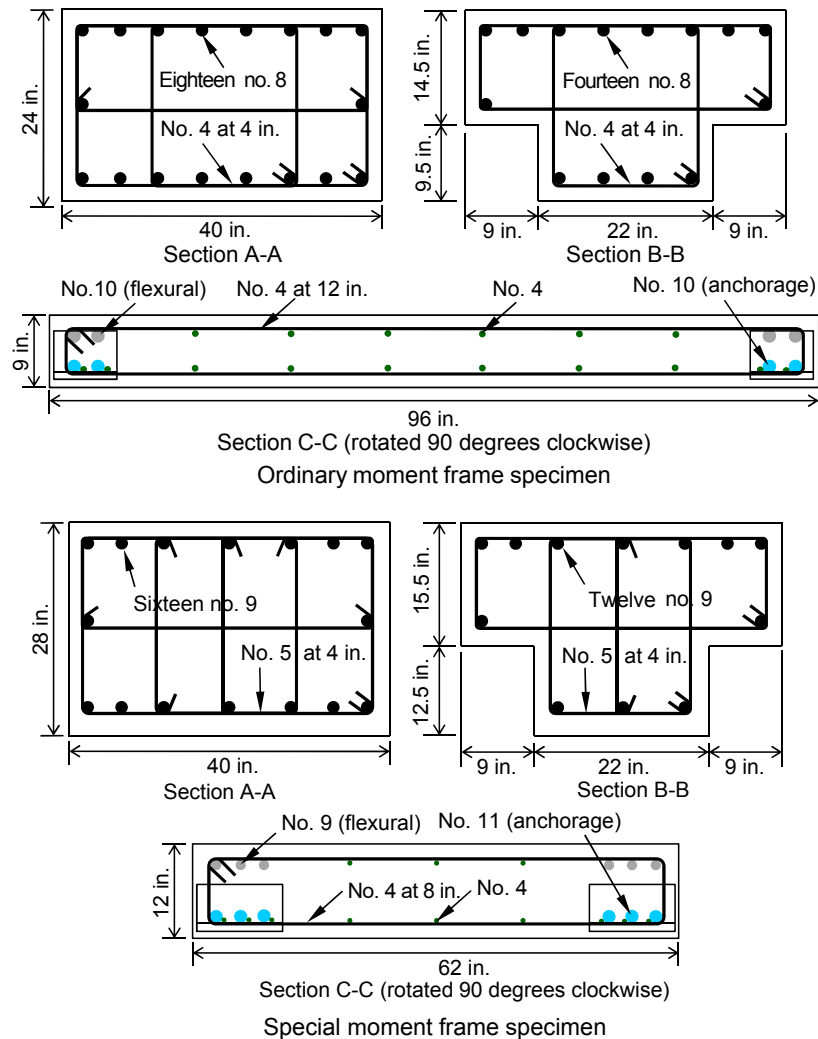
Figure 5. Member cross section and reinforcement details. Note: No. 4 = 13M; no. 5 = 16M; no. 8 = 25M; no. 9 = 29M; no. 10 = 32M; no. 11 = 36M; 1 in. = 25.4 mm.

attached to the reinforcing bars and anchorage bars in the beams, to the link plates connecting the beams and columns, and to the W16 × 67 (W410 × 100) beams used to brace the tops of the end columns.

Strain gauges on reinforcing bars and shear studs were installed at the precasting plant prior to concrete placement, while surface-mounted strain gauges on the link plates and brace beams were installed at the testing facility. Strain gauges on the anchorage bars were installed at locations where tensile forces were expected and were installed in pairs on opposite sides of the bars to enable measurement of flexure as well as axial strains in the bars.

The vertical load applied by the hydraulic actuator was measured by a load cell with a capacity of 400 kip (1800 kN). The estimated uncertainty in the measured load,

displacement, rotation, and strain data is ±1%. In addition to these measurements, three digital video cameras were used to record each test. A camera was aligned with each of the three columns to capture deformations, surface cracking, spalling, and component failure in the region surrounding each moment connection.

Experimental results for ordinary moment frame specimen

Observed behavior and failure modes

Figure 6 shows a plot of the applied vertical load versus the vertical displacement Δ of the center column for the ordinary moment frame specimen. **Figure 7** illustrates the progression of damage corresponding to the circled labels in Fig. 6. The load versus displacement was es-
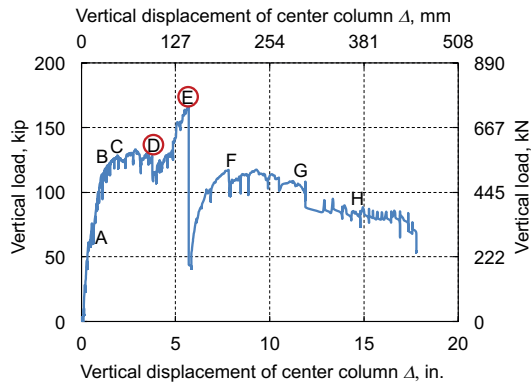
Figure 6. Applied vertical load versus vertical displacement of center column for ordinary moment frame specimen. Note: Labeled points D and E correspond to images in Fig. 7.

sentially linear up to point A, when concrete cracking occurred in the beams around the upper link plates at the center column and the stiffness of the specimen decreased. Further reductions in stiffness occurred at points B and C as concrete cracks formed in the end columns at the lower column plates. The load reached an initial peak of 133 kip (592 kN) at Δ equal to 2.87 in. (72.9 mm) and then began

to decrease. A drop in the load at point D was associated with detachment of the upper column plate from the left end column. The column plate was attached to the column with shear studs (Fig. 3), and detachment of the column plate was associated with concrete cracking on the left end column (Fig. 7). **Figure 8** shows another view of the cracking and spalling of concrete associated with detachment of the upper column plate from the left end column.

After the drop in load at point D in Fig. 6, the load began to increase steeply again up to point E, reaching an ultimate peak of 166 kip (738 kN) at Δ equal to 5.66 in. (144 mm). Between points D and E, the specimen developed additional capacity through arching action, with the top corner of each beam bearing against the center column and the bottom corner of each beam bearing against the end columns. Such bearing was evidenced by a narrowing of the gaps between the beams and columns with associated cracking and spalling of concrete in regions where bearing forces developed (Fig. 7).

After reaching the ultimate load at point E, the load dropped sharply to only 25% of its peak value. This drop in load was associated with fracture of the no. 10 (32M) anchorage bars welded to the bottom connecting angle on the left side of the center column. The anchorage bars fractured at the end of the flare-bevel-groove weld on the
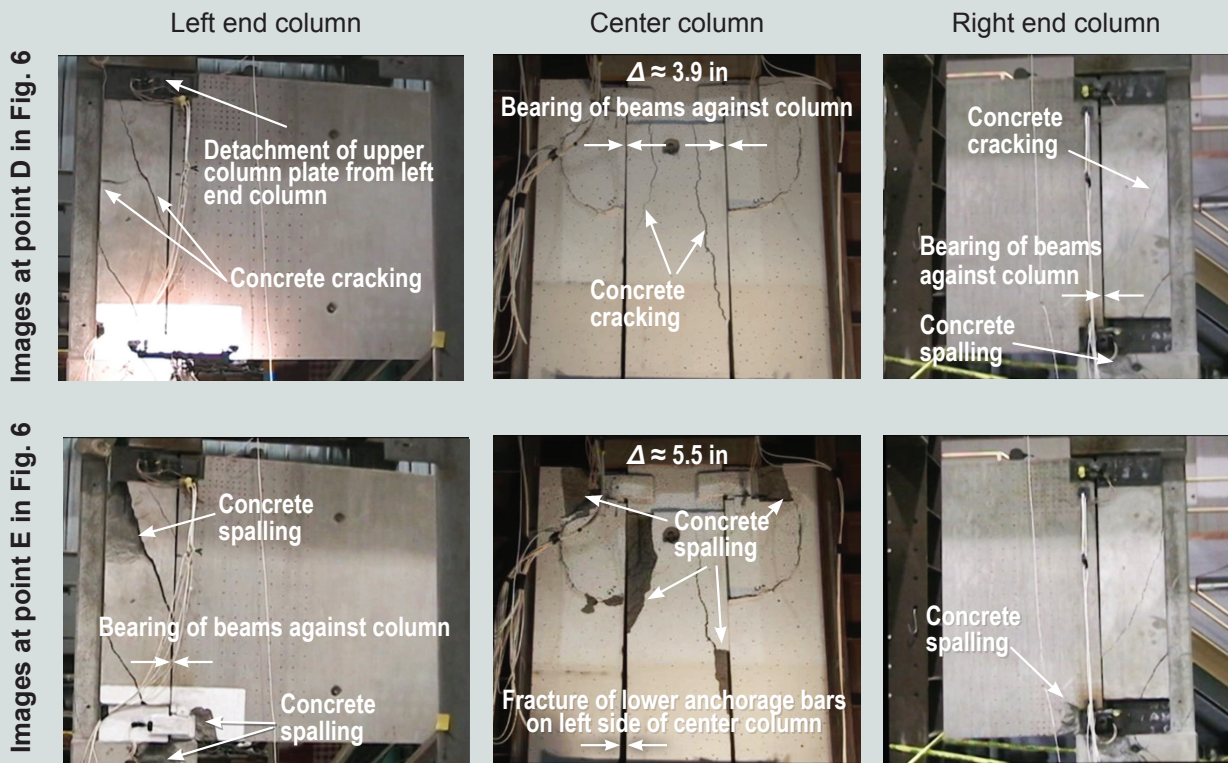
Figure 7. Progression of damage for ordinary moment frame specimen. Note: Images correspond to labeled points in Fig. 6.

Figure 8. Observed failure modes for ordinary moment frame specimen.

Detachment of upper column plate from left end column

Fractured anchorage bars from lower left connection to center column

Final damage to right end column

Upper link plate at right end column

Lower link plate at right end column

Eccentricity in force transfer

Resulting bending of link plate and anchorage bars
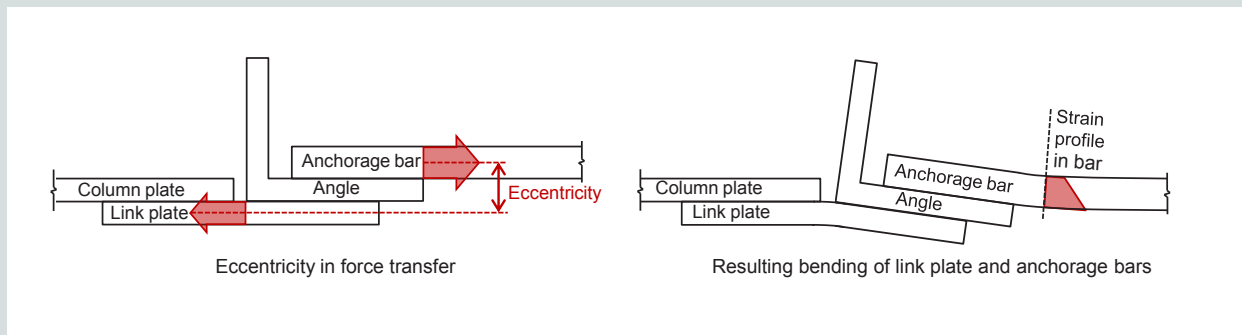
Figure 9. Top view of link plate connection illustrating eccentricity in force transfer and resulting bending of link plate and anchorage bars.

connecting angle (Fig. 3), as is evident in **Fig. 8**, which shows the connecting angle and welded anchorage bars recovered from the specimen after the test.

After fracture of the anchorage bars, the load increased steeply as the specimen developed additional resistance through arching action, reaching 70% of the ultimate load at point F. A drop in load at point F was associated with fracture of the lower torsion bar at the right end column accompanied by diagonal cracking and shear deformation of the right end column below beam level.

Shear deformation of the right end column continued throughout the remainder of the test, and Fig. 8 shows the final state of damage. Another drop in load at point G was associated with fracture of the lower torsion bar at the left end column accompanied by shear deformation of the left end column below beam level, which continued throughout the remainder of the test. Shear deformation of the left end column occurred with extensive concrete spalling. At point H in Fig. 6, the upper column plate detached from the right end column, similar to the failure observed previously on the left end column at point D. This failure was accom-

panied by cracking and spalling of concrete on the right end column. Large deformations of the link plates were observed (Fig. 8), which indicated extensive yielding. Out-of-plane bending of the link plates resulted from eccentricity in the transfer of forces through the link plate connections (**Fig. 9**). This eccentricity also resulted in bending of the anchorage bars, which contributed to their fracture, as discussed subsequently.

Figure 9 illustrates the bending that resulted from link plates in tension. For link plates in compression, the bending was reversed. (Compare the bending of the upper and lower link plates at the right end column in Fig. 8.) Finally, as the load continued to decrease and large chunks of concrete spalled from the specimen, the test was terminated at Δ equal to 17.8 in. (452 mm).

Displacement measurements

Figure 10 shows the displacement profile of the beams at selected values of the center column vertical displacement Δ. The displacement profile is largely symmetrical up to the ultimate load at Δ equal to 5.66 in. (144 mm), but
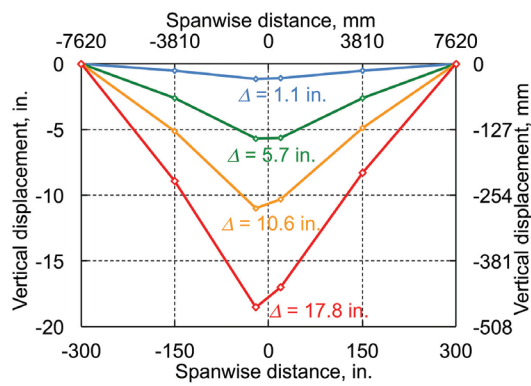
Figure 10. Vertical displacement profile of beams corresponding to indicated center-column displacements (ordinary moment frame specimen; displacements magnified). Note: Δ = vertical displacement. 1 in. = 25.4 mm.
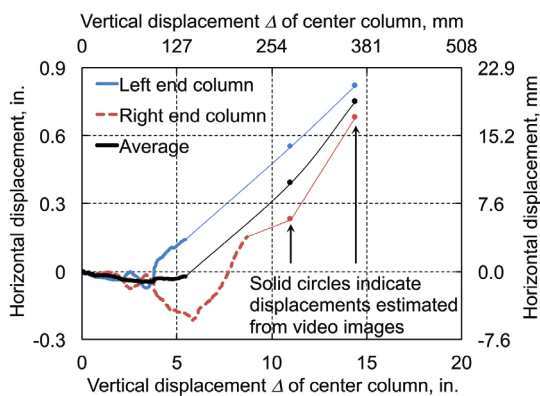
Figure 11. Horizontal displacement of end columns at beam midheight (ordinary moment frame specimen).
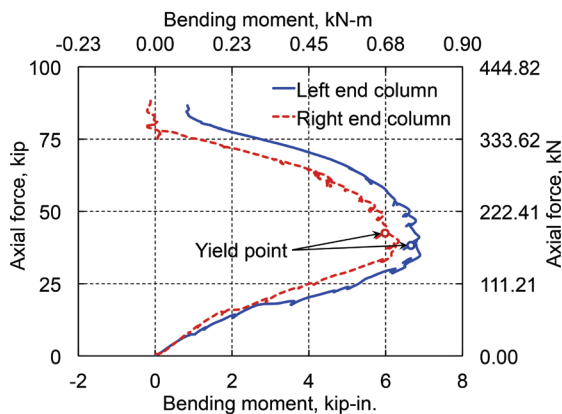
Figure 12. Axial force versus bending moment for upper anchorage bars at end columns (ordinary moment frame specimen). Note: 1 in. = 25.4 mm; 1 kip = 4.448 kN.

some asymmetry is evident after the ultimate load, with larger displacements on the left side of the center column than on the right side. This asymmetry resulted from the anchorage bar fractures on the lower left side of the center column. Measured rotations at the beam ends differed from the calculated beam chord rotation by about 0.20 degrees at most. This implies that the beams essentially rotated as rigid bodies, with most of the deformations localized at the beam-to-column connections.

Figure 11 shows the horizontal displacement of the end columns at beam midheight, with positive values signifying outward displacement, plotted against the vertical displacement of the center column. The average of the two measurements, which cancels out rigid-body motions, is also plotted for comparison. Initially, both end columns displaced slightly inward, reaching an average inward displacement of 0.044 in. (1.1 mm) prior to the onset of arching action. After the onset of arching action at Δ equal to 4.0 in. (100 mm) (point D in Fig. 6), both end columns displaced to the left by about 0.17 in. (4.4 mm), indicating a slight rigid-body rotation of the end columns, which were linked at their tops by brace beams (Fig. 4). During this rigid-body rotation, the average inward displacement decreased slightly as a result of arching action.

After fracture of the anchorage bars at Δ equal to 5.66 in. (144 mm) (point E in Fig. 6), the motion of the right column changed directions and both end columns moved outward. The measured displacement from both gauges froze at an outward displacement of about 0.15 in. (3.8 mm) and did not provide meaningful data after this point. Horizontal displacements after this point were estimated from video images, with an estimated uncertainty of ±0.1 in. (±2.5 mm) determined by comparing displacements obtained from the video images with those measured by the displacement gauges. The displacements estimated from the video images are shown as solid circles in Fig. 16 and indicate that both end columns continued to displace outward as a result of arching action. An average outward displacement of 0.75 in. (19 mm) was estimated at Δ equal to 14.4 in. (366 mm), which corresponds to point H in Fig. 6.

Measurements from strain gauges

Strain gauges were installed in pairs on the front and back sides of anchorage bars near the link plate connections, and these gauges enabled measurements of the bending that resulted from connection eccentricities (Fig. 9). At link plates subjected to tension, this bending was evidenced through tensile strains that were larger on the front of the bar than on the back (strain profile in Fig. 9). **Figure 12** presents an interaction diagram of axial force versus bending moment in the upper anchorage bars at the end columns. These axial force and bending moment values were calculated
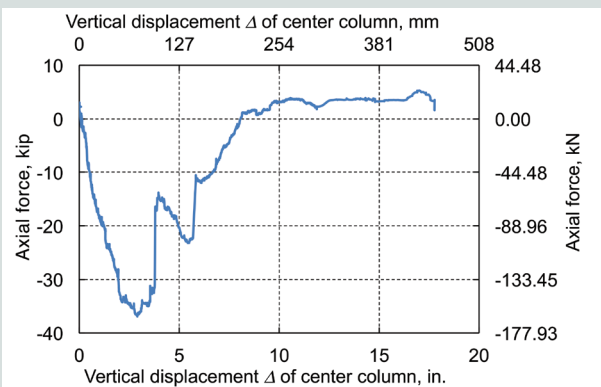
Figure 13. Axial force in front brace beam (ordinary moment frame specimen). Note: 1 kip = 4.448 kN.
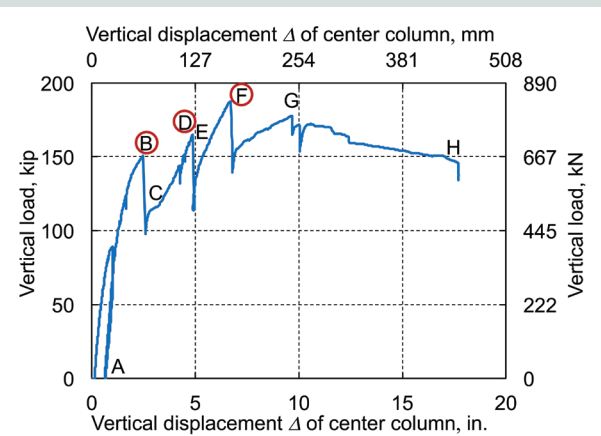
Figure 14. Applied vertical load versus vertical displacement of center column for special moment frame specimen. Note: Labeled points B, D, and F correspond to images in Fig. 15.

from the measured strains by assuming a linear strain profile across the bar (Fig. 9) using the measured stress-strain curve for a no. 10 (32M) bar (from tensile testing reported in NIST Technical Note 1886[13]) to calculate the corresponding stress profile and numerically integrating the stress profile over the cross section of the bar. Open circles on the curves of calculated bending moment and axial force indicate the point at which yielding first occurred on the front side of the bar. Based on tensile testing,[13] the yield capacity of a no. 10 (32M) bar was 81.3 kip (362 kN). Figure 12 thus shows that bending moments due to connection eccentricities caused yielding to initiate when the axial force was at about half of the yield capacity of the bar.

Figure 13 shows the axial force in the front brace beam spanning between the tops of the end columns, which was obtained from the average measured axial strain at midspan of the brace beam. Compressive forces developed

in the brace beam initially when the end columns moved inward at beam midheight (Fig. 11) and as negative moments in the beams tended to rotate the tops of the end columns inward. A drop in the compressive force at Δ equal to 3.7 in. (94 mm) corresponded to detachment of the upper column plate from the left end column, and a second drop at Δ equal to 5.7 in. (145 mm) corresponded to anchorage bar fracture. Tensile forces subsequently developed in the brace as the tops of the end columns were pushed outward by arching action.

Experimental results for special moment frame specimen

Observed behavior and failure modes

Figure 14 shows a plot of the applied vertical load versus the vertical displacement of the center column for the special moment frame specimen. **Figure 15** illustrates the progression of damage corresponding to circled labels in Fig. 14. The specimen was initially loaded to 89 kip (390 kN) and then unloaded to confirm that the instrumentation, data acquisition, and loading systems were working properly. During the initial phase of loading, some limited damage occurred, including concrete cracking on the right beam near the link plates. After unloading, the center column had a residual vertical displacement Δ of 0.65 in. (17 mm), corresponding to point A in Fig. 14. From this point, the specimen was loaded under monotonically increasing displacement for the remainder of the test.

After reaching an initial peak load of 151 kip (672 kN) at Δ equal to 2.49 in. (63.3 mm) (point B in Fig. 14), the vertical load dropped to 98 kip (435 kN). This drop in load was associated with fracture of a no. 11 (36M) anchorage bar welded to the bottom connecting angle on the left side of the center column (connection detail in Fig. 3). Strain data from the link plates indicated that the bottom anchorage bar fractured first and that the upper two anchorage bars fractured subsequently. The anchorage bars fractured at the end of the flare-bevel-groove weld on the connecting angle (**Fig. 16**).

After the drop in load at point B in Fig. 14, the load increased beyond the initial peak load, reaching a peak of 165 kip (735 kN) at point D before dropping sharply again at Δ equal to 4.88 in. (124 mm). Between points C and D, the specimen developed additional capacity through arching action, with the bottom corner of each beam bearing against the end columns and the top corner of each beam bearing against the center column. The drop in load at point D was associated with the fracture of the two remaining no. 11 (36M) anchorage bars welded to the bottom connecting angle on the left side of the center column. Fracture of these anchorage bars was evidenced by further
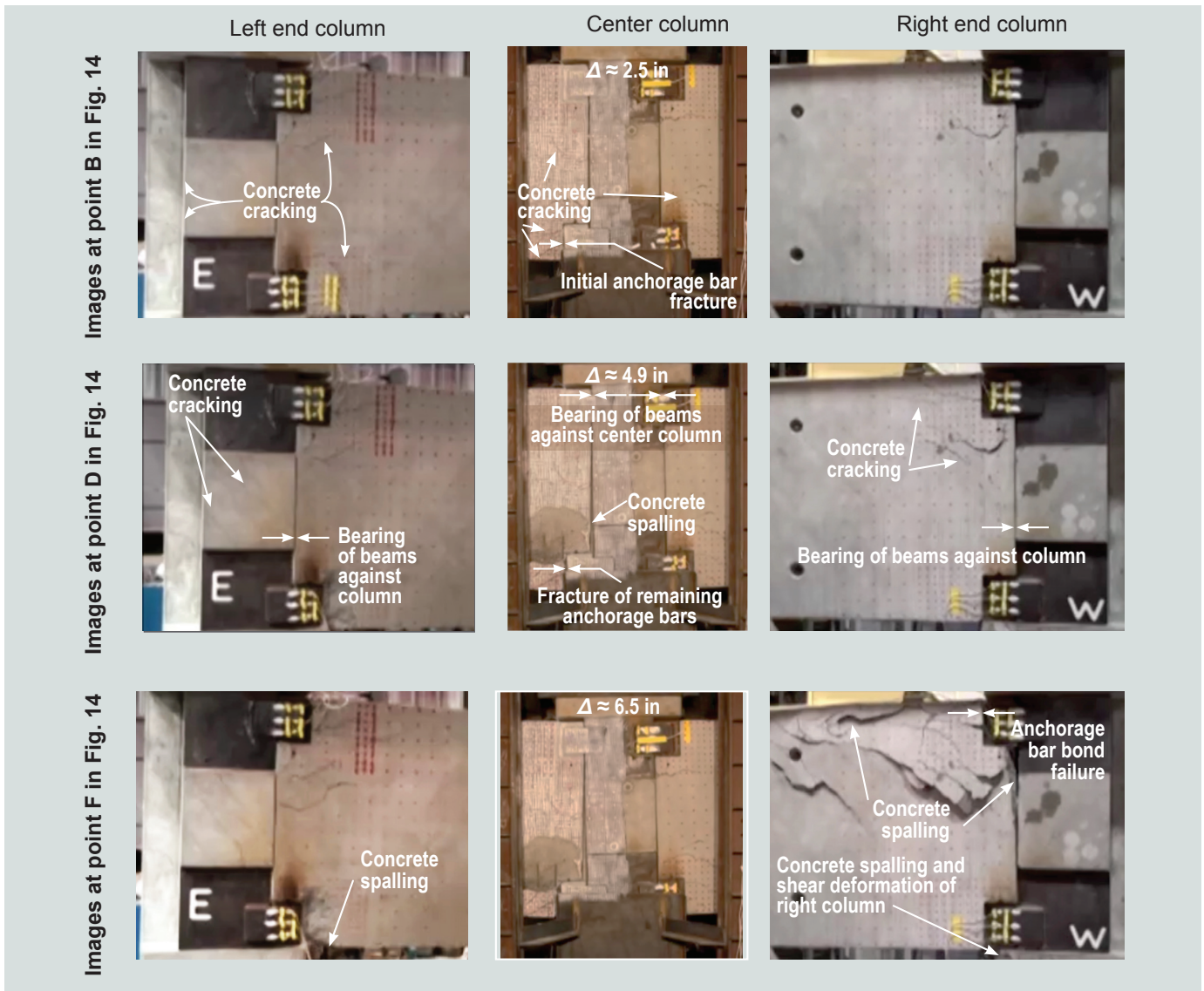
Figure 15. Progression of damage for special moment frame specimen. Note: Images correspond to labeled points in Fig. 14.

increases in the gap between the left beam and the center column, as well as extensive spalling of concrete near the anchorage bars (Fig. 15).

After the drop in load at point D in Fig. 14, the load increased again up to point F, reaching an ultimate peak load of 188 kip (836 kN) at Δ equal to 6.69 in. (170 mm). Between points E and F, the specimen continued to develop additional capacity through arching action. The sharp drop in load at point F was associated with bond failure of the upper anchorage bars at the right end column, resulting from the formation of splitting cracks and spalling of the concrete covering the upper anchorage bars near the right end column. Initial surface cracking was previously evident at this location (point E in Fig. 15). Finally, at point F, extensive spalling had occurred and a substantial gap had opened between the right beam and the right end column, providing evidence of bond failure (Fig. 15). A close-up photograph in Fig. 16 illustrates the splitting failure and concrete spalling that resulted in bond failure at this location. As indicated in Fig. 15, shear deformation of the right end column also commenced with the drop in load at point F accompanied by diagonal cracking and spalling of concrete below the beam level (Fig. 16). Shear deformation of the right end column continued throughout the remainder of the test.

After the drop in load at point F (Fig. 14), the load continued to increase, but with a reduced stiffness, reaching 95% of the ultimate load at point G. A drop in load at point G was associated with diagonal cracking of the left end column below the beam level (Fig. 16). Shear deformation of the left end column commenced at point G and continued throughout the remainder of the test. By the end of the test, both end columns had displaced noticeably outward below the beam level, as a result of arching action, while the tops

Fractured anchorage bars from lower left connection to center column

Splitting failure and spalling at upper anchorage bars at right end column

Diagonal cracking of right end column

Diagonal cracking of left end column

Figure 16. Observed failure modes for special moment frame specimen.

of both end columns, which were linked by brace beams (Fig. 4), had displaced noticeably to the right. The left end column thus displaced leftward near its base but rightward at its top, resulting in extensive tensile cracking on its left side (Fig. 16). From point G in Fig. 14, the load gradually decreased, falling to 78% of the ultimate load at point H. Finally, as the load continued to decrease and large chunks of concrete spalled from the specimen, the test was terminated at Δ equal to 17.8 in. (452 mm).

Displacement measurements

Figure 17 shows the displacement profile of the beams at selected values of the center-column vertical displacement Δ. The displacement profile is largely symmetrical up to the initial peak load at Δ equal to 2.49 in. (63.3 mm). Some asymmetry is evident after that point, with larger displacements on the left side of the center column than on the right side, as a result of the anchorage bar fractures on the lower left side of the center column. Figure 17 shows that the deflected profile of each beam was approximately linear at each level of loading, indicating that most of the deformations were localized at the beam-to-column connections, with the beams primarily rotating as rigid bodies.

Figure 18 shows the horizontal displacement of the end columns at beam midheight, with positive values signifying outward displacement, plotted against the vertical displacement of the center column. Figure 18 also shows the average of the two measurements, which cancels out rigid body motions. Initially, both end columns displaced slightly inward at beam midheight, reaching an average inward displacement of 0.042 in. (1.1 mm) prior to the onset of arching action. After fracture of the anchorage bars at Δ equal to 2.6 in. (66 mm) (point B in Fig. 14), both end columns began to move outward as a result of arching
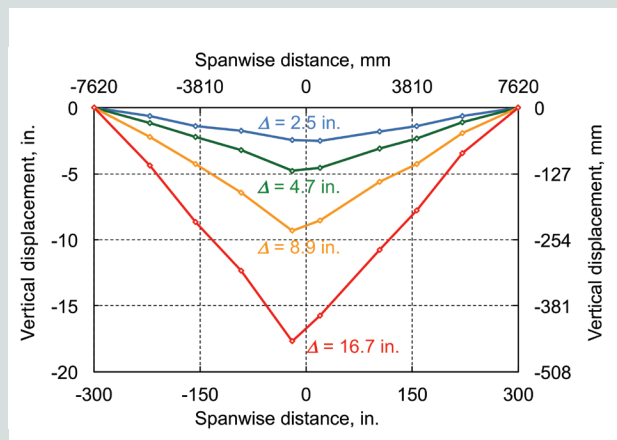
Figure 17. Vertical displacement profile of beams corresponding to indicated center-column displacements (special moment frame specimen; displacements magnified). Note: 1 in. = 25.4 mm.
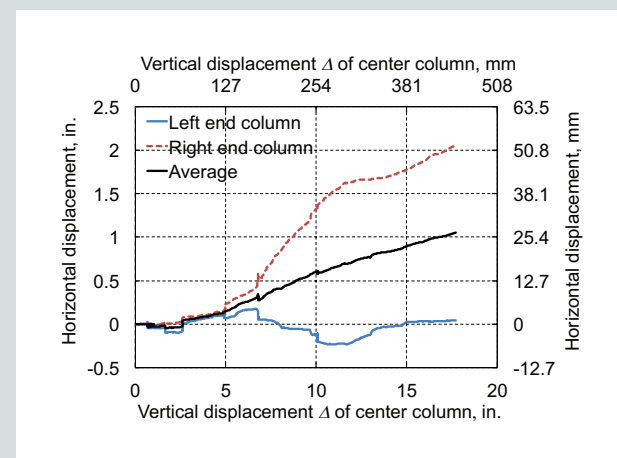
Figure 18. Horizontal displacement of end columns at beam midheight (special moment frame specimen).
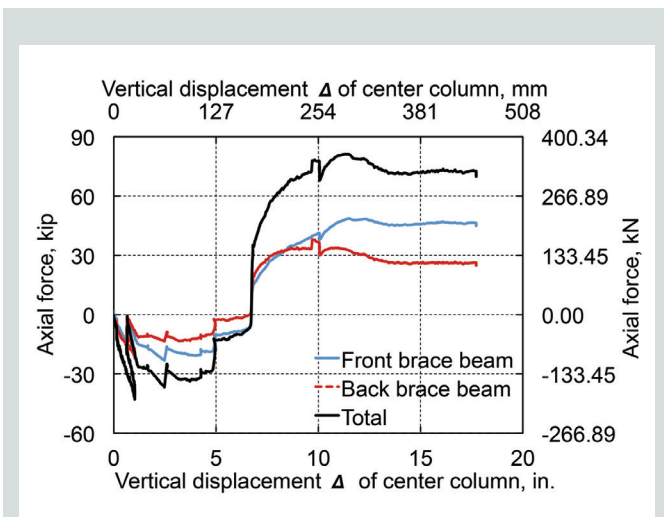
Figure 19. Horizontal displacement of end columns at beam midheight (special moment frame specimen).

action in the beams. At Δ equal to 6.7 in. (170 mm), after bond failure of the upper anchorage bars at the right end column, and after shear deformation of the right end column commenced (point F in Figure 14), the motion of the left column changed direction, and both columns moved to the right at beam midheight. The left column reached a peak inward (rightward) displacement of 0.23 in. (5.8 mm) at Δ equal to 11.7 in. (297 mm) before changing direction again and beginning to move outward as a result of cracking and shear deformation of the left column. Although the displacement of the left column changed directions due to rigid-body motions, the average displacement at beam midheight shows a monotonically increasing outward displacement after the onset of arching action, with an average outward displacement of 1.05 in. (26.7 mm) at the end of the test.

Measurements from strain gauges

Figure 19 shows the axial forces in the brace beams spanning between the tops of the end columns, which were obtained from the average measured axial strains at midspan of the brace beams. Figure 19 also shows the total brace force obtained by summing the axial forces in the two brace beams. Compressive forces developed in the brace beams initially when the end columns moved slightly inward at beam midheight (Fig. 18) and as negative moments in the beams tended to rotate the tops of the end columns inward. Sudden reductions in the compressive force in the brace beams at Δ equal to 2.5 in. (64 mm) and at Δ equal to 4.9 in. (120 mm) corresponded to fracture of the lower anchorage bars on the left side of the center column (Fig. 15). A steep reversal in the sign of the brace beam forces, from compressive to tensile, occurred at Δ equal to 6.7 in. (170 mm), which corresponded to bond failure of the upper anchor-

age bars at the right end column and the onset of shear deformations of the right end column (Fig. 15). The top of the right end column was subsequently forced outward (rightward) by arching action, pulling the top of the left end column rightward as well, and thus developing tensile forces in the brace beams.

Differences between the axial forces in the two brace beams resulted from torsion in the end columns. Because the precast concrete spandrel beams were aligned with the front faces of the columns, rather than their centerlines (top view in Fig. 4), forces in the link plates produced torsion in the end columns. This torsion was resisted by contact with the cross beams used to brace the end column tops at their inside and outside faces, resulting in differential forces in the front and back brace beams.

Initially, tensile forces in the upper link plates on the end columns tended to pull the front faces of the end columns inward, and this torsional rotation was resisted by greater compression in the front brace beam. Subsequently, compressive forces associated with arching action tended to push the front faces of the end columns outward, and this torsional rotation was resisted by greater tension in the front brace beam.

Conclusion

The responses of the two specimens consisted of three primary stages (**Fig. 20**). In the first stage, loads were resisted through flexural action. Tensile forces in the bottom link plates at the center column were balanced by compressive forces in the top link plates, and tensile forces in the top link plates at the end columns were balanced by compressive forces in the bottom link plates.

In the second stage, loads were resisted through a combination of flexural action and arching action. This stage began when deflections and rotations of the beams caused the initial gaps between the beams and columns to close, with the top corners of the beams bearing against the center column and the bottom corners of the beams bearing against the end columns, pushing them outward.

In the third stage, the specimens continued to carry loads through arching action but at a reduced capacity because of multiple failures that reduced the flexural resistance of the beam-to-column connections. Specifically, these failures degraded the capacity for transfer of tensile forces through the link plate connections, both at the upper link plates on the end columns and at the lower link plates on the center column. After the flexural resistance was compromised by these failures in the transfer of tensile forces, diagonal cracks and shear deformations developed in the lower portions of the end columns as continued arching action forced the end columns outward. Catenary action did not
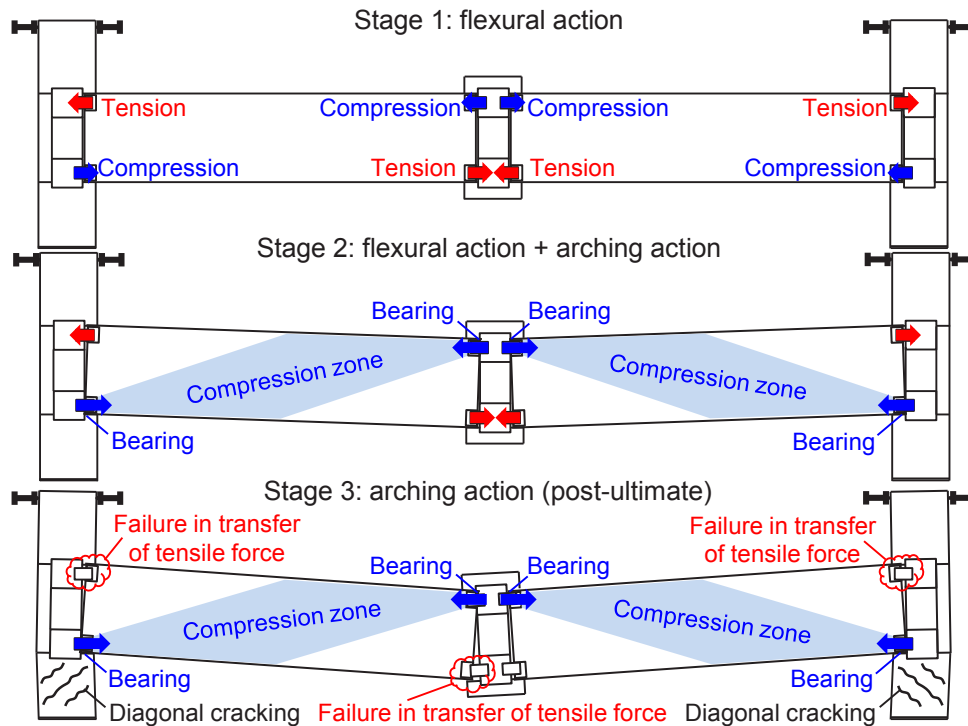
Figure 20. Three stages in the response of the precast concrete specimens.

develop in either the ordinary moment frame specimen or the special moment frame specimen, in contrast with previous testing of reinforced concrete moment frames,[5] for which tensile forces developed in the beams when the deflection of the center column was approximately equal to the beam depth. The precast concrete spandrel beams tested in this study had greater span-to-depth ratios than the reinforced concrete beams tested previously, and failures of the beam-to-column connections depleted the capacities of the specimens when the deflections of the center column remained much less than the beam depths.

Based on the study reported herein, the following observations and conclusions can be drawn:

- Both the ordinary moment frame and special moment frame specimens exhibited the following failure modes:

    – cracking and spalling of concrete near the welded link plate connections between the precast concrete beams and columns

    – fracture of the bottom anchorage bars at the welded connection to the center column

    – diagonal cracking, spalling, and outward shear deformation of the end columns below beam level as a result of arching action in the beams

- Fracture of the welded anchorage bars occurred at relatively small beam chord rotations of 0.019 rad for the ordinary moment frame specimen and 0.0087 rad for the special moment frame specimen. As a result of eccentricities in the connections (Fig. 9), the anchorage bars were subjected to local bending moments, which interacted with the tensile forces to produce larger tensile stresses.

- The diagonal cracking, spalling, and shear deformation of the end columns observed in these tests indicate that lateral forces due to arching action could potentially result in shear failure of columns. If arching action is to be exploited in resisting vertical loads under column removal scenarios, care must then be taken to ensure that the surrounding structure, including the columns and potentially the floor system, can resist the lateral loads induced by arching action.

- Additional failure modes that were observed included the following:

    – detachment of embedded steel column plates with welded shear studs from the end columns of the

ordinary moment frame specimen under a combination of unbalanced shear forces and out-of-plane bending induced by the link plates

– bond failure of the upper anchorage bars at the right end column at the ultimate load of the special moment frame specimen, resulting from the formation of splitting cracks and spalling of concrete

• The ultimate capacity of the ordinary moment frame specimen was 166 kip (738 kN), while the ultimate capacity of the special moment frame specimen was 188 kip (836 kN). Corresponding beam chord rotations at the ultimate load were 0.019 rad for the ordinary moment frame specimen and 0.022 rad for the special moment frame specimen. Thus, the more stringent seismic design requirements for the special moment frame specimen resulted in an increase of only 13% in the ultimate capacity under the column removal scenario, with an increase of 18% in the corresponding beam chord rotation.

The companion paper[6] presents computational modeling of the precast concrete moment frame specimens and provides conclusions regarding their performance under column removal scenarios.

Acknowledgments

References

1. Griffiths, H., A. G. Pugsley, and O. Saunders. 1968. *Report of the Inquiry into the Collapse of Flats at Ronan Point, Canning Town*. Ministry of Housing and Local Government. London, UK: Her Majesty's Stationery Office.

2. Delatte, N. J. 2009. *Beyond Failure: Forensic Case Studies for Civil Engineers*. Reston, VA: ASCE Press.

3. Elliott, K. S., and C. K. Jolly. 2013. *Multi-Storey Precast Concrete Framed Structures*. 2nd ed. West Sussex, UK: Blackwell Publishing.

4. Sadek, F., J. A. Main, H. S. Lew, S. D. Robert, V. P. Chiarito, and S. El-Tawil. 2010. *An Experimental and Computational Study of Steel Moment Connections under a Column Removal Scenario*. NIST (National Institute of Standards and Technology) Technical Note 1669. Gaithersburg, MD: NIST.

5. Lew, H. S., Y. Bao, F. Sadek, J. A. Main, S. Pujol, and M. A. Sozen. 2011. *An Experimental and Computational Study of Reinforced Concrete Assemblies under a Column Removal Scenario*. NIST Technical Note 1720. Gaithersburg, MD: NIST.

6. Bao, Y., J. A. Main, H. S. Lew, and F. Sadek. 2017. "Performance of Precast Concrete Moment Frames Subjected to Column Removal: Part 2, Computational Analysis." *PCI Journal* 62 (5): 53–74.

7. Regan, P. E. 1974. *Catenary Tests on Composite Precast–In Situ Concrete Composite Floors*. Report to the Department of Environment. London, UK: The Polytechnic of London.

8. Shultz, D., E. Burnett, and M. Fintel. 1978. *A Design Approach to General Structural Integrity –Design and Construction of Large Panel Concrete Structures*. Supplemental report A. Skokie, IL: Portland Cement Association.

9. Engström, B. 1990. "Connections between Precast Components." *Nordisk Betong, Journal of the Nordic Concrete Federation* 2 (3): 53–56.

10. Nimse, R. B., D. D. Joshi, and P. V. Patel. 2014. "Behavior of Wet Precast Beam Column Connections under Progressive Collapse Scenario: An Experimental Study." *International Journal of Advanced Structural Engineering* 6 (4): 149–159.

11. Nimse, R. B., D. D. Joshi, and P. V. Patel. 2015. "Experimental Study on Precast Beam Column Connections Constructed Using RC Corbel and Steel Billet under Progressive Collapse Scenario." *Structures Congress 2015 Proceedings, April 23–25, 2015, Portland, Oregon*. Reston, VA: ASCE.

12. Kang, S. B., and K. H. Tan. 2015. "Behaviour of Precast Concrete Beam–Column Sub-assemblages Subject to Column Removal." *Engineering Structures* 93: 85–96.

13. Main, J. A., Y. Bao, H. S. Lew, F. Sadek, V. Chiarito, S. D. Robert, and J. Torres. 2015. *An Experimental and Computational Study of Precast Concrete Moment Frames under a Column Removal Scenario*. NIST Technical Note 1886. Gaithersburg, MD: NIST.

14. AWS (American Welding Society). 2010. *Structural Welding Code—Steel*. AWS D1.1/D1.1M:2010. Miami, FL: AWS.

15. ACI (American Concrete Institute). 2005. *Building Code Requirements for Structural Concrete (ACI 318-05) and Commentary (ACI 318R-05)*. Farmington Hills, MI: ACI.

16. PCI Industry Handbook Committee. 2004. *PCI Design Handbook: Precast and Prestressed Concrete*. MNL-120. 6th ed. Chicago, IL: PCI.

17. ASCE (American Society of Civil Engineers). 2005. *Minimum Design Loads for Buildings and Other Structures*. SEI/ASCE 7-05. Reston, VA: ASCE.

18. ASTM International. 2016. *Standard Specification for Deformed and Plain Low-Alloy Steel Bars for Concrete Reinforcement*. ASTM A706/A706M-16. West Conshohocken, PA: ASTM.

19. ASTM International. 2008. *Standard Specification for Carbon Structural Steel*. ASTM A36/A36M-08. West Conshohocken, PA: ASTM.

20. ASTM International. 2016. *Standard Specification for Alloy-Steel and Stainless Steel Bolting for High Temperature or High Pressure Service and Other Special Purpose Applications*. ASTM A193/A193M-16. West Conshohocken, PA: ASTM.

Notation

d_b = reinforcing bar diameter

f_y = yield strength

L = span length between column centerlines

t_w = throat dimension of flare-bevel-groove weld

Δ = vertical displacement

About the authors

H. S. Lew, PE, PhD, is a senior research engineer in the Engineering Laboratory at the National Institute of Standards and Technology (NIST). He received his PhD from the University of Texas at Austin. He is an Honorary Member of ACI and has served on the ACI Board of Direction and Technical Activities Committee. He is a member of ACI Committee 318, Concrete Research Council, and other ACI committees. His research interests include the performance of structural members and systems, construction safety, failure investigations, and earthquake engineering.

Joseph Main, PhD, is a research structural engineer in the Engineering Laboratory at NIST. He received his PhD from Johns Hopkins University in Baltimore, Md. His research interests relate to the computational assessment of structural performance under extreme loads, including wind loading, air-blast loading, and loading generated by abnormal events, such as fire, explosions, and vehicular impacts.

Yihai Bao, PhD, is an Intergovernmental Personnel Act researcher in the Engineering Laboratory at NIST. He received his BS and MS degrees from Tongji University in China and his PhD from the University of California, Davis. His research interests include nonlinear modeling of structural behavior under extreme loading conditions, large-scale experimental methods, and advanced scientific computational methods.

Fahim Sadek, PE, PhD, is a research structural engineer in the Engineering Laboratory at NIST. He received his PhD from the Southern Methodist University in Dallas, Tex. His research interests include the vulnerability of structures subjected to multihazard conditions, the response of structures to dynamic and impulse loading, and structural health monitoring.

Vincent P. Chiarito, PE, MASCE, FSEI, is a research structural engineer in the Geotechnical and Structures Laboratory at the U.S. Army Engineer Research and Development Center in Vicksburg, Miss. For over 34 years, he has conducted vibration, earthquake, and blast effect studies to support structural engineering research for civil and military projects and a variety of government and private-sector customers. He is a subject matter expert in the Department of Defense on blast, shock, impact, disproportionate collapse, bridge and tunnel security, and testing and evaluation for structural health monitoring.

Stephen D. Robert, MS, is a research civil engineer in the Geotechnical and Structures Laboratory at the U.S. Army Engineer Research and Development Center in Vicksburg, Miss. His research includes blast-resistant design and analysis of structures, weapon effects research, and structural vulnerability to progressive collapse. He holds an MS in civil engineering from Mississippi State University in Starkville. He is an associate member of the American Society of Civil Engineers (ASCE) and serves on the ASCE Structural Engineering Institute's Blast, Shock, and Impact Committee.
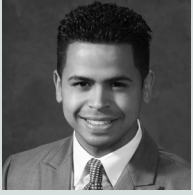
Jorge O. Torres-Alamo, BS, is a research civil engineer in the Geotechnical and Structures Laboratory at the U.S. Army Engineer Research and Development Center in Vicksburg, Miss. He has more than six years of research experience focused primarily on evaluating and protecting critical U.S. infrastructure and military assets. His most recent national contributions were the experimental validation of a mitigation scheme intended for the protection of cast-iron structures and structural vulnerability studies of thin-arch concrete dams. He received a bachelor's degree in civil engineering from the University of Puerto Rico at Mayaguez.

Abstract

This paper presents a full-scale experimental study of two precast concrete moment-frame assemblies, each comprising three columns and two beams. The assemblies represented portions of seismically designed perimeter moment frames from two 10-story proto-type buildings. One assembly was part of an ordinary moment frame, and the other was part of a special moment frame. The assemblies were subjected to monotonically increasing vertical displacement of the unsupported center column to observe their behavior and failure modes under simulated column removal.

The failures of both the ordinary moment frame and special moment frame specimens were character-ized by fracture of the bottom anchorage bars at the welded connection to the center column and diagonal cracking and shear deformation of the end columns under outward forces generated by arching action in the beams.

Additional failure modes included shear stud failure for the ordinary moment frame specimen and bond failure of anchorage bars for the special moment frame specimen.

Keywords

Review policy

This paper was reviewed in accordance with the Precast/Prestressed Concrete Institute's peer-review process.

Reader comments

Please address reader comments to journal@pci.org or Precast/Prestressed Concrete Institute, c/o *PCI Journal*, 200 W. Adams St., Suite 2100, Chicago, IL 60606. ⌐